Structure of a two-dimensional superparamagnetic system in a quadratic trap

F. Yang and W. Kong*
College of Science, Civil Aviation University of China, Tianjin 300300, China

S. F. Liu† and C. Z. Wang
School of Physics, Nankai University, Tianjin 300071, China

(Received 14 August 2020; accepted 12 October 2020; published 23 October 2020)

Ground-state structures of a two-dimensional (2D) system composed of superparamagnetic charged particles are investigated by means of molecular dynamics simulation. The charged particles trapped in a quadratic potential interact with each other via the repulsive, attractive, and magnetic dipole-dipole forces. Simulations are performed within two regimes: a one-component system and a two-component system where the charged particles have the identical charge-to-mass ratio. The effects of magnetic dipole-dipole interaction, mixing ratio of the two species and confinement frequency on the ground-state structures are discussed. It is found that as the strength of the magnetic dipole increases, the charged particles tend to self-organize into chainlike structures. The two species particles exhibit different structural features, depending on the competition of electrostatic repulsive interaction, magnetic dipole-dipole interaction and confinement force. The potential lanes are observed through analyzing the global potential of the magnetic particles, which guide the unmagnetic particles aligning themselves in the direction of the potential lanes.

DOI: 10.1103/PhysRevE.102.043213

I. INTRODUCTION

Colloidal matter or dusty plasma contains nanometer to millimeter sized particles immersed in a weakly ionized plasma environment. It is an ideal platform to study the self-organization phenomena of the strongly coupled system [1–14]. Of special interest are the ground-state structures of the two-dimensional (2D) finite system [15–19], which provides a potential candidate for the design of microstructures used in the nanotechnology [20,21] and materials processing [22–24]. So far, it has been clear that the competition of the interaction forces determines the various structures of the system. In this paper, we attempt to identify the effects of magnetic dipole-dipole interaction on the ground-state structures of the charged particles trapped in a quadratic potential, by emphasizing the binary mixture system. Charged particles doping with the ferromagnetic materials such as Fe_3O_4 or γ Fe_2O_3 can acquire magnetic dipole moment, and form the magnetic particles in the presence of external magnetic field [25]. The magnetic dipole-dipole interaction is usually anisotropic and can be repulsive or attractive depending on the orientation of the magnetic dipole [26–29]. Previous studies on the superparamagnetic colloidal crystals have shown that the stable crystal lattices including triangular, rectangular, oblique, chainlike oblique, and rhombic structures can be formed at zero temperature [30,31], where the mutual interaction between the colloids is governed by magnetic dipole-dipole force and a short-ranged repulsion. Hartmann *et al.* extended this study to 2D dusty plasma crystals [32], in which the interparticle spacing is typically on the order of 100 μm, falling in the range of terahertz (THz) wavelengths. They found that the lattice spacing can be tuned by changing the external magnetic field, where the charged dust particles interact with each other via magnetic dipole-dipole force and repulsive screened Coulomb force. Normally, the attractive force in the colloids (characterized by the second term of Lennard-Jones potential) or the attractive potential in the dusty plasma (due to the thermionic electron emission and dust shadowing) is omitted, for its weakness as compared to the repulsive counterpart. However, previous studies have found that the attractive force also contributes to the formation of ordered structures such as voids, shells, and clusters [16,19,33–42]. It will be, thus, of interest to make clear that how does the magnetic dipole-dipole interaction operate in a more realistic system to affect the ground-state structures. Intuitively, the ordered structures should be distorted when the anisotropic magnetic dipole-dipole interaction is sufficiently strong, on the other hand, the details are far from fully understood, to the best of our knowledge.

In this study, we first give the preliminary results based on the one-component system. Then, the focus is moved to the system composed of two-component superparamagnetic charged particles, since more physics are expected therein [43–48]. In the colloidal suspensions, the monolayer can be reached by confining the particles on a liquid-gas interface, while in the dusty plasma, the identical charge-to-mass ratio for each particle is required to satisfy the force balance perpendicular to the horizontal 2D plane. Here, we assume the particles have the same charge-to-mass ratio. Actually, the 2D or quasi-two-dimensional (Q2D) dusty plasma

*wkong@cauc.edu.cn
†lsfnku@nankai.edu.cn

with two species particles has been achieved in recent laboratory experiments [14,49,50], thus the results herein hopefully are detectable. This work also serves as a reference for the quenching of a multicomponent suparamagnetic fluid, where the slow dynamics and structural relaxation undergo before the system reaches the ground state. Depending on the complexity of the fluid and the quenching depth, the system may either crystallize or remain in an amorphous state [51]. The manuscript is arranged as follows: Sec. II gives the simulation model in detail. Simulation result and discussion are presented in Sec. III. Section IV is devoted to a conclusion.

II. SIMULATION MODEL

The magnetic charged particles exposed to an uniform magnetic field receive the following forces: horizontal confinement force, long-ranged repulsive force, short-ranged attractive force, and magnetic dipole-dipole force. The Lorentz force due to the external magnetic field is not considered since it is rather small as compared to the others in our simulation, more importantly, the equilibrium structure of the system is independent of the uniform magnetic field based on the Bohr–Van Leeuwen theorem [52,53]. Then, the equation of motion for the particles moving at 2D (x-y) plane is given by

$$m_i\frac{\mathrm{d}^2\mathbf{r}_i}{\mathrm{d}t} = -\nabla\left(\sum_i^N \frac{m_i\omega^2}{2}\mathbf{r}_i^2 + \sum_{i\neq j}^N \Phi_R + \sum_{i\neq j}^N \Phi_A + \sum_{i\neq j}^N \Phi_M\right) + \zeta_i(t), \tag{1}$$

where m_i and $\mathbf{r}_i$, respectively, are the mass and coordinate of ith particle, and ω is the trap frequency. The last term at the rhs of Eq. (1), as a thermostat, is used to anneal the system until the ground state is reached, i.e., the kinetic energy K is much smaller than the potential energy U of the system. The gradually decreasing temperature $T(t)$ of the system relates to the stochastic thermal kick $\zeta(t)$ according to the fluctuation-dissipation theorem [54–59]

$$\langle\zeta_i(0)\zeta_i(t)\rangle = 2m\nu k_B T(t)\delta(t), \tag{2}$$

where ν is the collision frequency between the charged particles and the ambient medium, k_B is the Boltzmann constant, and δ is the Dirac delta function. In our simulation, each run is initialized at a high temperature $T = 0.1 \to 1$, the time step is $0.002\omega_{pd}^{-1}$, the number of annealing cycles is 5×10^7, and K/U is on the order of 10^{-6} or less at the end of the annealing. Repulsive potential energy Φ_R, attraction potential energy Φ_A and magnetic dipole-dipole potential energy Φ_M, respectively, are expressed as

$$\Phi_R = \frac{Q_iQ_j}{r}\exp(-\kappa r), \tag{3}$$

$$\Phi_A = -B\exp(-\beta r), \tag{4}$$

$$\Phi_M = \frac{M^2}{r^3}(1-3\cos^2\alpha\cos^2\theta). \tag{5}$$

In Eq. (2), Φ_R takes the form of Yukawa potential, where Q is the charge of the particle, r is the interparticle distance, and

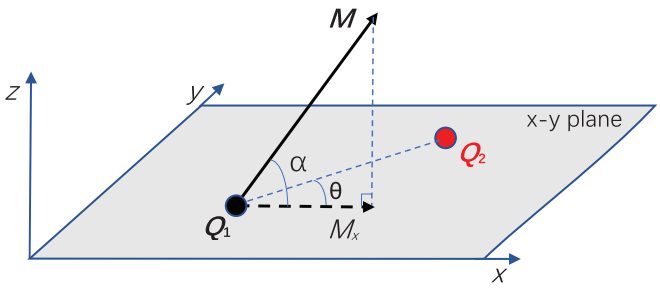

FIG. 1. Sketch of a pair of superparamagnetic particles Q_1 and Q_2. Magnetic moment $\mathbf{M}$ for both of the magnetic particles is aligned to the external magnetic field. The tilt angle of $\mathbf{M}$ with respect to the 2D (x-y) plane is α. The project of $\mathbf{M}$ onto the 2D plane, i.e., M_x, is assumed to be along the x direction without losing generality. The angle between M_x and connection vector of the pair particles is θ.

$\kappa = a/\lambda_D$ is the screening coefficient with a being Wigner-Seitz radius and λ_D being Debye radius. In Eq. (3), B is the attraction strength, and β characterizes the screening length. In Eq. (4), M is the magnitude of the magnetic dipole moment, which is proportional to the magnitude of the external magnetic field. More discussion about M is given in our previous study [29]. α and θ, respectively, denote the direction of magnetic dipole moment and the relative orientation of the pair particles, as sketched in Fig. 1.

Units are used throughout the paper unless otherwise stated, which are length is normalized by $a = (n\pi)^{-1/2}$, where n is the areal number density for the overall particles. Time is normalized by $\omega_p^{-1} = [2Q_1^2/(a^3m_1)]^{-1/2}$. Energy is normalized by $U_0 = Q_1^2/a$. In the simulation, Q_1 and m_1 are fixed, while Q_2 and m_2 are varied.

To characterize the strength of the magnetic dipole-dipole interaction, we employ a dimensionless parameter

$$\eta = (M^2/a^3)\big/\big(Q_1^2/a\big), \tag{6}$$

which is the ratio of the magnetic dipole-dipole interaction energy (with $\alpha = 90^\circ$) to the bare Yukawa potential energy (i.e., the screened cloud of the charged particles is removed) of a pair of charged particles with distance a. η ranges from 0 to 1 based on the typical dusty plasma parameters (for example [32], $T_e = 2$ eV, $n_i = 10^{10}\mathrm{cm}^{-3}$, the radius of dust particle is 5μm, the particle surface potential is 2V, the magnetic field varies from 0 to 1 T).

III. SIMULATION RESULT AND DISCUSSION

The simulations are arranged as follows: in subsection A, the charged particles are assumed to have the identical charge and mass, i.e., one-component system. The ground-state structures with high asymmetry are discussed. In subsection B, the charged particles are classified into two species, i.e., species 1 and species 2. The difference in the charge and mass is quantified by the parameter $\mu = Q_2/Q_1 = m_2/m_1$. The proportion of the species 1 particles is given by $x_1 = N_1/N$, where N_1 and N, respectively, are the number of species 1 particles and total particles. In subsection C, we briefly discuss the connection between simulation and dusty plasma experiment, particularly for the two-component system.

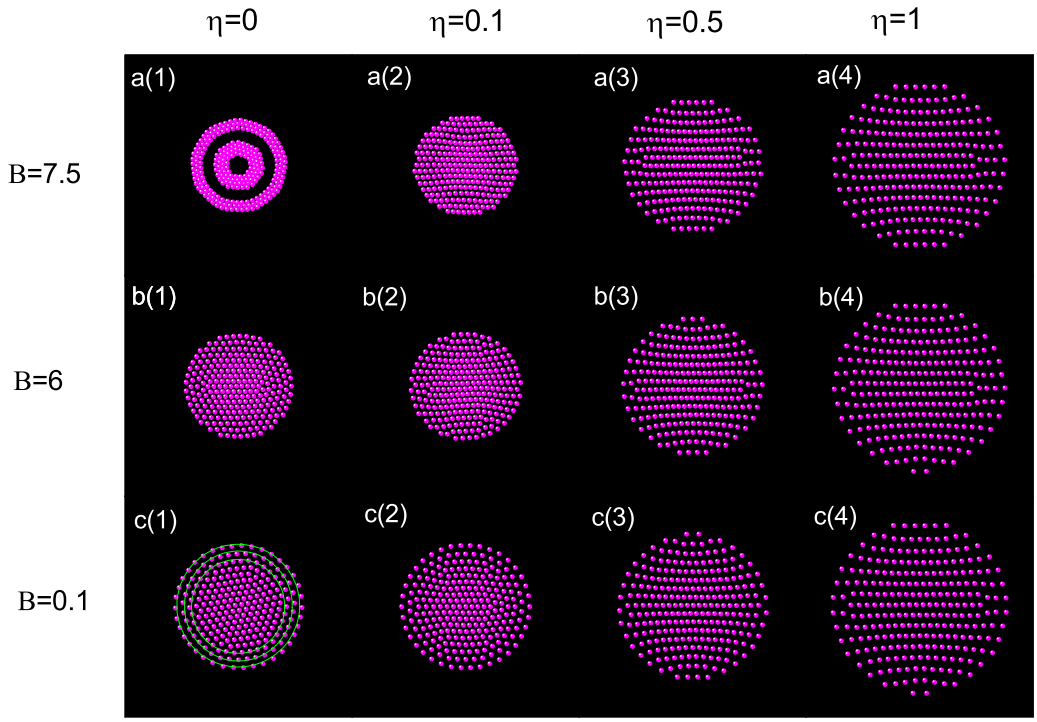

FIG. 2. Configurations of the one-component system with $N = 256$ and $\alpha = 60^\circ$. In the columns, attraction strength B is decreased from the top to the bottom. In the rows, magnetic dipole strength η is increased from the left to the right. Three shells in the panel c(1) are indicated with the green lines.

A. One-component system

In the previous study [19], Liu *et al*. have shown a wealth of ground-state structures based on the molecular dynamics simulation, where the magnetic dipole-dipole interaction is absent. As a benchmark, also for the further investigation, we carry out the simulations with some parameters therein.

Figure 2 shows the ground-state structures of the system with $\kappa = 0.9$, $\beta = 4.0$, $\alpha = 60^\circ$ and $N = 256$. The effects of magnetic dipole strength η and attraction strength B are investigated. In panel a(1) of Fig. 2, the circular shells with inner voids are self-organized with $\eta = 0$, which agree well with result shown in Fig. 3 of Ref. [19]. When η is present (even for a very small $\eta = 0.1$), the ordered structures are broken up, instead, the 2D ball appears. When η is further increased, as shown in a(3) and a(4) of Fig. 2, the 2D ball expands as a result of the increasing repulsive magnetic dipole-dipole interaction. The resultant chainlike structures are consistent with the findings of Ref. [32], here the bending of the chains reflects the competition of the local magnetic dipole-dipole forces. When $\eta = 0$ and B is decreased, as shown in a(1), b(1), and c(1) of Fig. 2, one finds that the circular shells with inner voids also are broken up, then replaced by circular shells with inner hexagon crystals. The same phenomenon can be found in the case of $\eta = 0.1$, as shown in a(2), b(2) and c(2) of Fig. 2. When η is sufficiently strong, only the chainlike structure can be observed. To conclude, the system with a strong magnetic dipole-dipole interaction is most likely to self-organize into the chainlike structure. The attraction force contributes to the specific structures such as voids, circular shells and hexagon crystals.

Figure 3 shows the ground-state structures of the system with $\kappa = 0.9$, $\beta = 4.0$, $\eta = 1$ and $N = 256$. The effects of magnetic dipole direction α and attraction strength B are investigated. It is found that the chainlike structures are gone when α is increased gradually. This is straightforward since

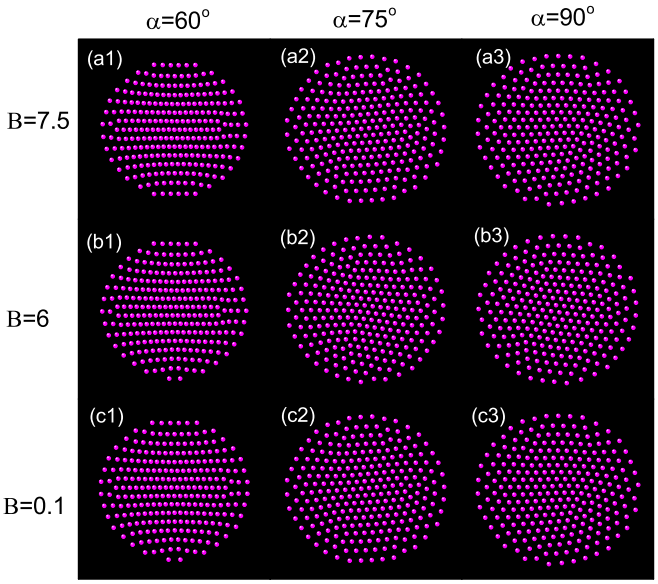

FIG. 3. Configurations of the one-component system with $N = 256$ and $\eta = 1$. In the rows, the chainlike structures are replaced by the circular shells with inner hexagon crystals with increasing α. In the columns, the structures basically remain unchanged with decreasing B.

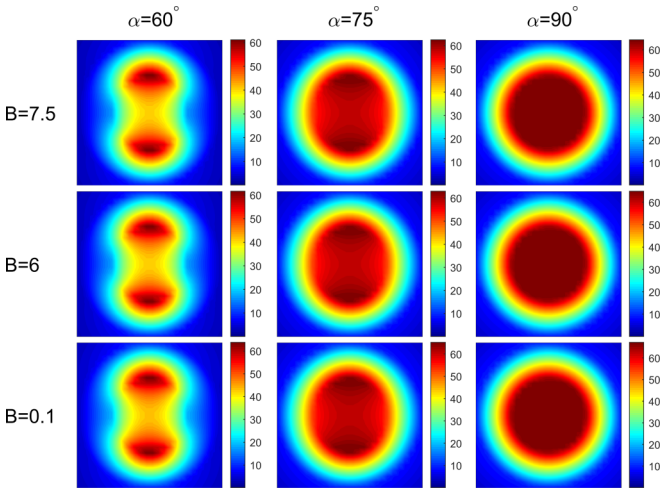

FIG. 4. Contours of the interaction potential (combination of Φ_R, Φ_A and Φ_M) for one charged particle. With increasing α, the potential tends to be radically asymmetric. For each column, the potential is independent of B. $\kappa = 0.9$, $\beta = 4$, and $\eta = 1$.

the anisotropy of the magnetic dipole tends to be weak when α is increased. Particularly for $\alpha = 90^\circ$, the trapped charged particles interact with each other via the isotropic potential (radial asymmetry) and the Wigner-like crystallization is formed. In the columns, the structures basically are not changed with changing B, since the magnetic dipole-dipole interaction is strong enough to dominate over the attraction force.

To verify Fig. 3, the interaction potential around one charged particle is plotted in Fig. 4. As expected, the potentials with the smaller α have a stronger anisotropy, and the wells are (light regions) along the x direction. This leads to the chainlike structures as shown in the panels a(1), b(1) and c(1) of Fig. 3. Meanwhile, the potentials with the same α are independent of B, showing that the magnetic dipole-dipole interaction indeed dominates over the attraction interaction. Here we note that α ranges from 60° to 90° in order to avoid the aggregation of the charged particles [29,32].

Figure 5 shows the effects of ω and η on the ground-state configurations. According to Refs. [60,61], the ground-state configurations of the system do not depend on the confinement ω. The theory goes like this: although ω participates in the calculation of the potential energy term of the Hamiltonian, it just defines the absolute values of the energy and the cluster size. The configurations of the minimum energy is determined only by the particle number N. Here we include all of Φ_R, Φ_A, Φ_M and the confinement potential to investigate the dependence. $N = 20$ is chosen because a fine configuration with it can be observed in the dusty plasma experiment [61] (12 and 7 particles are on the first and second rings, respectively, with a central particle). It is shown the ground-state configurations in panels a(1), b(1), and c(1) of Fig. 5 indeed are not affected by ω, meanwhile, the cluster shrinks when ω increases, being consistent with the above theory. We have also examined the case of $\eta \neq 0$, as shown in the second and third columns of Fig. 5. The subtle changes in the particle number and direction of the chains can be observed, nevertheless, the ground-state configurations do not depend on ω basically.

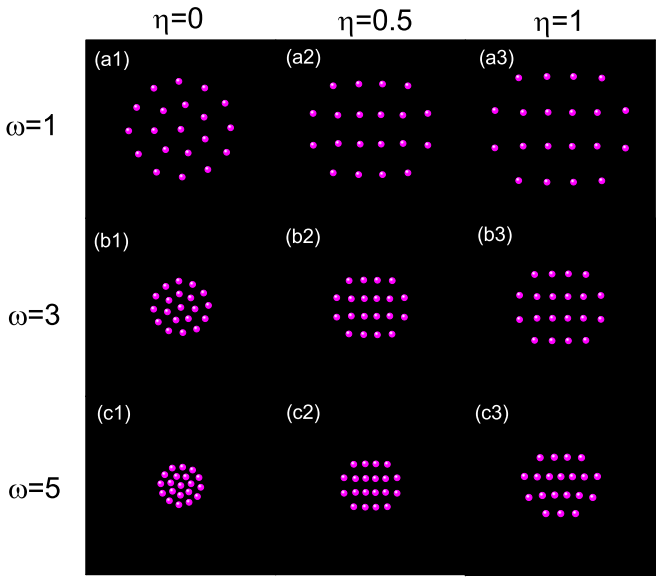

FIG. 5. Configurations of the one-component system with $N = 20$. In the columns, the cluster size is decreased with increasing ω, which has no influence on the ground-state configurations. In the rows, the chainlike structures tend to appear with increasing η and the 2D balls expand. $\kappa = 1$, $B = 0.1$, $\beta = 3$, and $\alpha = 60^\circ$.

B. Two-component system

In this section, we extend the aforementioned study to the two-component system. First, the ground-state configurations with different mixing ratio of the two species are investigated in Fig. 6, where $\mu = 2$, $\kappa = 1$, $B = 6$, $\beta = 3$, $\alpha = 60^\circ$, and $N = 64$. It is found that (i) In the first column, where $\eta = 0$, the species 2 particles (red ones) are in the outer region, by contrast, the species 1 particles (green ones) condense to a core located at the central region. This does make sense since the species 2 particles have more charges, thereby they are pushed out due to the stronger repulsive interaction Φ_R. (ii) Again in the first column, the number of the outer rings is decreased with increasing x_1, and the cluster size shrinks due

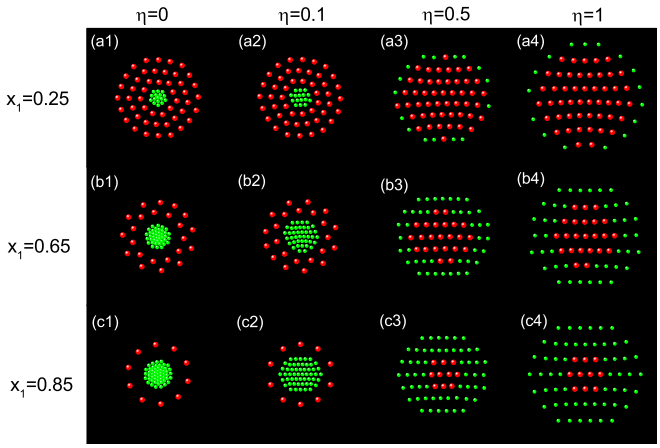

FIG. 6. Configurations of the two-component system with $N = 64$ and $\alpha = 60^\circ$. In the columns, proportion of the species 1 particles x_1 is increased from the top to the bottom. In the rows, magnetic dipole strength η is increased from the left to the right.

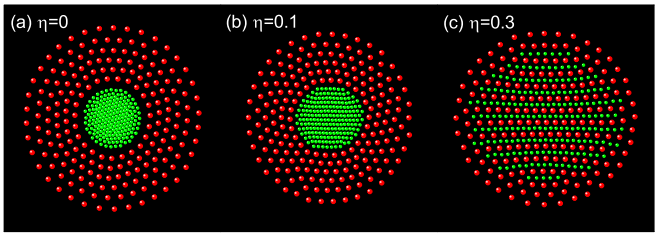

FIG. 7. Configurations of the two-component system with $N = 400$, $x_1 = 0.5$, and $\mu = 2$. The species 1 particles (green ones) are magnetic and the species 2 particles (red ones) are unmagnetic.

to the decreasing of the effective repulsive attraction Φ_R. (iii) When a smaller η is present (second column), the species 1 particles self-organize into the chainlike configuration, while the species 2 particles remain in the ring configuration. When η is increased further (third and fourth columns), the species 2 particles also self-organize into the chainlike structures. These results reflect the competition of Φ_M and Φ_R, i.e., both species 1 and species 2 particles exhibit chainlike structures when Φ_M dominates over Φ_R. (iv) The most interesting point is that the species 1 particles tend to move outward in the regime of Φ_M ($\eta = 0.5, 1$), which is right opposite to those of the first two columns. We give the explanation as follows: the previous study has shown that the lattice spacing increases as η increases for $\alpha > \alpha_{th}$ [32]. That will result in a considerable decline of the repulsive interparticle forces, including the contributions of Φ_R and Φ_M. When η is big enough, the confinement force begins to play an important role in determining the position of the particles. Considering the confinement force is proportional to m (mass of the charge particles), thus the particles with smaller m receive less confinement force and they tend to move outward.

In the two-component system, there is an interesting question that how does the charged particles arrange themselves when some unmagnetic particles get involved in. Figure 7 shows the ground-state configurations of such a system, where the species 1 particles are magnetic and the species 2 particles are not. The parameters are $\kappa = 1.5$, $B = 7.5$, $\beta = 4$, and $\alpha = 60^\circ$. It is found that the species 1 particles (magnetic particles) tend to form the chainlike configurations and move outward as η increases. Surprisingly, the species 2 particles (unmagnetic particles) also form the chainlike configurations when η is strong enough ($\eta = 0.3$). This result is robust and independent of μ, x_1 and N. Recalling Φ_M is anisotropic, here we infer that the magnetic particles collectively generate the potential lanes in the x direction, which guide the unmagnetic particles aligning themselves in chains as well.

In order to verify the above inference, we calculate the superposition of Φ_R and Φ_M of the species 1 particles based on the parameters of Fig. 7. The corresponding global potential in the real space is mapped, as shown in Fig. 8. It is found that when $\eta = 0$, the global potential of the species 1 particles is radially isotropic. However, the global potential tends to be anisotropic as η increases, particularly for panel (c) of Fig. 8, where the global potential is dominated by Φ_M and the potential lanes along the x direction are formed, which result in the alignment of the unmagnetic particles.

At last, the effects of ω on the ground-state configurations of the two-component system are investigated, as shown in Fig. 9. The system is composed of the unmagnetic particles with $\mu = 2, \kappa = 1, B = 6, \beta = 3$. A perfect structure of two rings with a central particle is self-organized. One finds that the global configurations of the system are independent of ω, being consistent with the conclusion of Fig. 5. However, the outer ring moves inward and the inner ring nearly keeps still as ω increases. This is easy to understand since the particles with bigger mass (red ones) receive a bigger change of the confinement force when ω is varied, while the electrostatic interaction is unchanged because of the fixed μ.

C. Connection between simulation and dusty plasma experiment

Ordered structures of monodisperse charged particles trapped in a well have been observed in the dusty plasma experiments, including the two-dimensional hexagons [5,6], two-dimensional voids [62], three-dimensional nested shells [63,64], etc. It is a popular idea that the competition among the screened Coulomb interaction, confinement and other forces determines the final states. In this study, the anisotropic magnetic dipole-dipole interaction is taken into account and the chainlike structure tends to be formed when Φ_M is sufficiently strong. Recalling the studies on the structure of magnetic particles in the dusty plasma experiments with magnetic field [26,27], where the chainlike structure along the magnetic field has been observed, the simulations shown here make sense.

Here we note the simulation of two-component system, where the interesting phenomena such as location exchange of species 1 and species 2 particles and chainlike alignment of nonmagnetic particles are observed. To verify them in the two-dimensional binary mixture dusty plasma experiment,

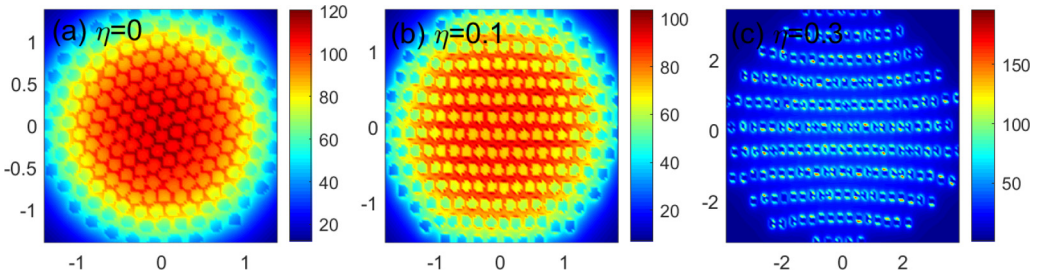

FIG. 8. Global potential distribution of the species 1 particles. In panel (a), only Φ_R of the species 1 particles exist in the real space. In panels (b) and (c), Φ_M of species 1 particles is added in and the potential lanes appear, particularly for the bigger η.

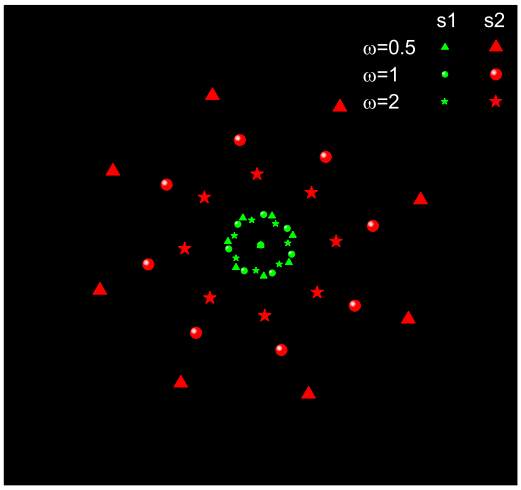

FIG. 9. Configurations of the two-component system with $N = 16$, $x_1 = 0.5$, $\mu = 2$, and $\eta = 0$. The species 1 particles (green ones) nearly keep still, while the species 2 particles (red ones) move inward as ω increases.

two species particles with different radius have to be prepared in advance. Normally, inert materials such as melamine formaldehyde, polymethyl methacrylate, and SiO_2 are used to manufacture the microparticles. Based on the analysis of Wieben *et al.* [49], the ratio of particle radii of the two species is limited to $1.07 \leqslant b_1/b_2 \leqslant 1.33$ because of the few available particle material, where $b_1/b_2 = (\rho_2/\rho_1)^{1/2}$ with ρ_1 and ρ_2 being the mass densities of the two species particles, respectively. We propose that the particles doping with ferromagnetic material may considerably increase the limit of b_1/b_2 (thus m_1/m_2 and Q_1/Q_2) because of the larger mole mass of Fe_3O_4 (or γ Fe_2O_3) relative to that of inert materials such as SiO_2. As for the magnetic dipole-dipole interaction, an adjustable magnetic field should be deployed in the dusty plasma experiment.

IV. CONCLUSION

In this paper, we have used a molecular dynamics simulation to investigate the ground-state structures of superparamagnetic charged particles. The structural properties of one-component and two-component systems are discussed, by changing the strength and direction of magnetic dipole moment, mixing ratio of the two species, and confinement strength. It is found that the chainlike structure is most likely to be self-organized when the magnetic dipole is strong enough (by increasing the magnitude of external magnetic field or choosing appropriate particle material). The competition of Φ_R, Φ_M, and ω determines interesting phenomena including: (1) In the regime of Φ_R, the particles with more charges tend to locate at the outer region due to the stronger electrostatic repulsive interaction. (2) In the regime of Φ_M, the particles with less mass tend to move outward due to the weaker confinement force. (3) In the moderate regime (for example, $\eta = 0.1$ in our simulation), the particles with less charges self-organize into the chainlike configuration, while the particles with more charges does not. For the coexistence of magnetic particles and unmagnetic particles, the potential lanes may appear in the system when η is strong enough, which lead to the alignment of the unmagnetic particles. These results are helpful to understand the structures of superparamagnetic charged particles trapped in a quadratic potential, particularly for the binary mixture system.

ACKNOWLEDGMENTS

This work is supported by National Natural Science Foundation of China under Grants No. 11805272 and No. 11505286, National Key R&D Program of China under Grant No. 2017YFE0301700, Civil Aviation University of China under Grants No. 3122013D001 and No. 3122013C009. Simulations are performed on TH-1A of National Supercomputer Center in Tianjin.

[1] K. Nelissen, B. Partoens, and F. M. Peeters, Phys. Rev. E **71**, 066204 (2005).
[2] H. Löwen, E. C. Oguz, L. Assoud, and R. Messina, Adv. Chem. Phys. **148**, 225 (2011).
[3] V. E. Fortov, A. V. Ivlev, S. A. Khrapak, A. G. Khrapak, and G. E. Morfill, Phys. Rep. **421**, 1 (2005).
[4] G. E. Morfill and A. V. Ivlev, Rev. Mod. Phys. **81**, 1353 (2009).
[5] H. Thomas, G. E. Morfill, V. Demmel, J. Goree, B. Feuerbacher, and D. Möhlmann, Phys. Rev. Lett. **73**, 652 (1994).
[6] J. H. Chu and L. I, Phys. Rev. Lett. **72**, 4009 (1994).
[7] B. Liu, Y. H. Liu, Y. P. Chen, S. Z. Yang, and L. Wang, Chin. Phys. B **12**, 765 (2003).
[8] W. Yang, Minghui Kong, M. V. Milošević, Zhi Zeng, and F. M. Peeters, Phys. Rev. E **76**, 041404 (2007).
[9] W. Kong, S. F. Liu, Q. L. Wang, B. L. Hu, and L. Wang, J. Phys. A **40**, 1171 (2007).
[10] Z. Donko, P. Hartmann, and G. J. Kalman, J. Phys.: Conf. Ser. **162**, 012016 (2009).
[11] E. Thomas Jr., B. Lynch, U. Konopka, R. L. Merlino, and M. Rosenberg, Phys. Plasmas **22**, 030701 (2015).
[12] W. Kong, F. Yang, S. F. Liu, and F. Shi, Phys. Plasmas **23**, 103705 (2016).
[13] E. Thomas Jr., U. Konopka, R. L. Merlino, and M. Rosenberg, Phys. Plasmas **23**, 055701 (2016).
[14] D. Block and A. Melzer, J. Phys. B **52**, 063001 (2019).
[15] Y. H. Liu, Z. Y. Chen, M. Y. Yu, L. Wang, and A. Bogaerts, Phys. Rev. E **73**, 047402 (2006).
[16] Y. H. Liu, Z. Y. Chen, M. Y. Yu, and A. Bogaerts, Phys. Rev. E **74**, 056401 (2006).
[17] L. Assoud, R. Messina, and H. Löwen, J. Chem. Phys. **129**, 164511 (2008).
[18] J. D. Feldmann, G. J. Kalman, P. Hartmann, and M. Rosenberg, Phys. Rev. Lett. **100**, 085001 (2008).
[19] Y. H. Liu, L. Y. Chew, and M. Y. Yu, Phys. Rev. E **78**, 066405 (2008).
[20] K. Ostrikov, Rev. Mod. Phys. **77**, 489 (2005).
[21] F. Bresme and M. Oettel, J. Phys.: Condens. Matter. **19**, 413101 (2007).
[22] J. W. Swan, J. L. Bauer, Y. Liu, and E. M. Furst, Soft Matter **10**, 1102 (2014).

[23] X. Tang, B. Rupp, Y. Yang, T. D. Edwalds, M. A. Grover, and M. A. Bevan, ACS Nano **10**, 6791 (2016).
[24] X. Tang, J. Zhang, M. A. Bevan, and M. A. Grover, J. Process Control **60**, 141 (2017).
[25] V. V. Yaroshenko, G. E. Morfill, D. Samsonov, and S. V. Vladimirov, IEEE Trans. Plasma Sci. **32**, 675 (2004).
[26] M. Puttscher and A. Melzer, New J. Phys. **16**, 043026 (2014).
[27] D. Samsonov, S. Zhdanov, G. Morfill, and V. Steinberg, New J. Phys. **5**, 24 (2003).
[28] P. Hartmann, Z. Donkó, M. Rosenberg, and G. J. Kalman, Phys. Rev. E **89**, 043102 (2014).
[29] F. Yang, S. F. Liu, W. Kong, and Y. L. Li, Phys. Plasmas **26**, 113701 (2019).
[30] V. A. Froltsov, R. Blaak, C. N. Likos, and H. Lowen, Phys. Rev. E **68**, 061406 (2003).
[31] L. Assoud, R. Messina, and H. Löwen, Europhys. Lett. **80**, 48001 (2007).
[32] P. Hartmann, M. Rosenberg, G. J. Kalman, and Z. Donkó, Phys. Rev. E **84**, 016409 (2011).
[33] T. Eckert and E. Bartsch, Phys. Rev. Lett. **89**, 125701 (2002).
[34] K. Ito, H. Yoshida, and N. Ise, Science **263**, 66 (1994).
[35] K. N. Pham, A. M. Puertas, J. Bergenholtz, S. U. Egelhaaf, A. Moussaïd, P. N. Pusey, A. B. Schofield, M. E. Cates, M. Fuchs, and W. C. K. Poon, Science **296**, 104 (2002).
[36] A. C. H. Coughlan, I. T. Díaz, J. Zhang, and M. A. Bevan, J. Chem. Phys. **150**, 204902 (2019).
[37] D. Samsonov and J. Goree, Phys. Rev. E **59**, 1047 (1999).
[38] X. Wang and A. Bhattacharjee, Phys. Plasmas **7**, 3093 (2000).
[39] J. Goree, G. E. Morfill, V. N. Tsytovich, and S. V. Vladimirov, Phys. Rev. E **59**, 7055 (1999).
[40] V. N. Tsytovich, S. V. Vladimirov, G. E. Morfill, and J. Goree, Phys. Rev. E **63**, 056609 (2001).
[41] Y. Liu, Y. Song, and Z. X. Wang, Phys. Plasmas **14**, 094501 (2007).
[42] Y. H. Liu, Z. Y. Chen, F. Huang, M. Y. Yu, L. Wang, and A. Bogaerts, Phys. Plasmas **13**, 052110 (2006).
[43] Y. Feng, J. Goree, and B. Liu, Phys. Rev. Lett. **100**, 205007 (2008).
[44] C. R. Du, V. Nosenko, S. Zhdanov, H. M. Thomas, and G. E. Morfill, Europhys. Lett. **99**, 55001 (2012).
[45] G. J. Kalman, P. Hartmann, Z. Donkó, K. I. Golden, and S. Kyrkos, Phys. Rev. E **87**, 043103 (2013).
[46] T. Ott, H. Löwen, and M. Bonitz, Phys. Rev. E. **89**, 013105 (2014).
[47] C. Killer, T. Bockwoldt, S. Schütt, M. Himpel, A. Melzer, and A. Piel, Phys. Rev. Lett. **116**, 115002 (2016).
[48] S. Schütt, M. Himpel, and A. Melzer, Phys. Rev. E **101**, 043213 (2020).
[49] F. Wieben, J. Schablinski, and D. Block, Phys. Plasmas **24**, 033707 (2017).
[50] C. R. Du, V. Nosenko, H. M. Thomas, Y. F. Lin, G. E. Morfill, and A. V. Ivlev, Phys. Rev. Lett. **123**, 185002 (2019).
[51] L. Berthier and G. Biroli, Rev. Mod. Phys. **83**, 587 (2011).
[52] T. A. Kaplan and S. D. Mahanti, Europhys. Lett. **87**, 17002 (2009).
[53] B. Savoie, Rev. Math. Phys. **27**, 1550019 (2015).
[54] R. K. Pathria, *Statistical Mechanics* (Pergamon Press, Oxford, 1972).
[55] W. F. van Gunsteren and H. J. C. Berendsen, Mol. Phys. **45**, 637 (1982).
[56] Yan Feng, Bin Liu, and J. Goree, Phys. Rev. E **78**, 026415 (2008).
[57] B. A. Klumov and G. E. Morfill, JETP Lett. **90**, 444 (2009).
[58] F. Yang, W. Kong, S. F. Liu, F. Shi, and Y. P. Wang, Phys. Plasmas **24**, 063702 (2017).
[59] W. Kong, S. F. Liu, F. Yang, F. Shi, and Y. P. Wang, Phys. Plasmas **25**, 083709 (2018).
[60] V. M. Bedanov and F. M. Peeters, Phys. Rev. B **49**, 2667 (1994).
[61] A. Melzer, *Introduction to Colloidal (Dusty) Plasmas*, Chap. 8, Lecture Notes in Physics (Springer, Berlin, 2016).
[62] R. P. Dahiya, G. V. Paeva, W. W. Stoffels, E. Stoffels, G. M. W. Kroesen, K. Avinash, and A. Bhattacharjee, Phys. Rev. Lett. **89**, 125001 (2002).
[63] O. Arp, D. Block, A. Piel, and A. Melzer, Phys. Rev. Lett. **93**, 165004 (2004).
[64] M. Bonitz, D. Block, O. Arp, V. Golubnychiy, H. Baumgartner, P. Ludwig, A. Piel, and A. Filinov, Phys. Rev. Lett. **96**, 075001 (2006).